

Title Page (with Author Details)

Property Analysis of β -Tetragonal Bismite Thin Films: Varied Concentrations and Enhanced Photocatalytic Efficiency

Hella Houda¹, Guettaf Temam Elhachmi¹, Mohammed Althamthami^{*1}, Hachemi Ben
Temam¹, Saâd Rahmane¹

¹*Physics Laboratory of Thin Layers and Applications, Biskra University, BP 145 RP,
Biskra 07000, Algeria*

*Corresponding author. (**Mohammed Althamthami**)

Tel.: +1 (604) 616 7293

E-mail.: mohammednasser132@gmail.com ; mohammed.althamthami@univ-biskra.dz ; mohammed.althamth1@ucalgary.ca

ORCID.: 0000-0003-1622-9662

Acknowledgements

The authors would like to thank the Algerian Directorate General for Scientific Research and Technological Development-DGRSDT for financial assistance.

Authors wish to thank Mr. Saâd Rahmane and Mr. Brahim Gasmi for his assistance in XRD data acquisition from (LPCMA), University of Biskra, Algeria and Pr. Tibarmacine from the University of Biskra, Algeria.

Property Analysis of β -Tetragonal Bismite Thin Films: Varied Concentrations and Enhanced Photocatalytic Efficiency

Abstract

In this study, we thoroughly examine β - Bi_2O_3 thin films as potential photocatalysts. We produced these films using an environmentally friendly Sol Gel method that is also cost-effective. Our research focuses on how different precursor concentrations, ranging from 0.1 M to 0.4 M, affect the photocatalytic performance of these films. We conducted a comprehensive set of tests to analyze various aspects of the films, including their structure, morphology, topography, optical properties, wettability, and photocatalytic capabilities. These tests provided us with a well-rounded understanding of the films' characteristics. To assess their photocatalytic efficiency, we used Methylene Blue (MB) as a contaminant and found that the films, particularly those with a 0.1 M concentration, achieved an impressive 99.9% degradation of MB within four hours. The 0.1 M film had a crystalline size of 39.7 nm, an indirect band gap of 2.99 eV, and a contact angle of 51.37° . Our findings suggest that β - Bi_2O_3 films, especially the 0.1 M variant, have promising potential for treating effluents from complex industrial dye processes. This research marks a significant step in utilizing sustainable materials to address pollution and environmental remediation challenges.

Keywords: Bismuth oxide; Dip coating; photocatalysis; Thin Films; Wettability.

1. Introduction

Organic dyes pose a considerable threat to environmental contamination [1–3]. They exhibit high levels of toxicity and can be hazardous when released into the environment, posing risks to aquatic organisms, humans, plants, and animals [4]. Therefore, it is crucial to implement effective treatment of these textile effluents before their discharge into the environment [5]. Out of the numerous techniques at hand, photocatalytic technology emerges as one of the foremost and highly effective methods for the elimination of organic dyes [6,7].

In this procedure, the degradation of pollutants in water is achieved by utilizing a catalyst composed of semiconductor nanoparticles and a radiation source. Typically, ultraviolet radiation is employed, although certain studies explore the utilization of solar radiation [8], which is the reagent of choice for the process of photocatalysis due to its abundance, low cost, and environmentally friendly nature [9]. Many semiconductors such as face centered ZnO [10], CdS, MoS₂, ZrO₂ [11], and TiO₂, were used for photocatalysis [12]. Among them, Bi₂O₃ nano-structured thin films have been proven to be valuable photo-catalyst [13]. Bismuth oxide has many advantages, including a large energy bandgap ranging from (2 to 3.96 eV) [14], also has a high refractive index and dielectric permittivity [15]. Bi₂O₃ generally exhibits six crystallographic phases viz α -Bi₂O₃ (monoclinic), β -Bi₂O₃ (tetragonal), γ -Bi₂O₃ (body-centered cubic), δ -Bi₂O₃ (face-centered cubic), ϵ -Bi₂O₃ (orthorhombic), and ω -Bi₂O₃ (triclinic) [16].

Moreover, heat of the stable low-temperature polymorph α -Bi₂O₃ results in the formation of the δ -Bi₂O₃ phase at about 730 °C, which, melts at roughly 825 °C. However, two transitions can occur during cooling: δ -Bi₂O₃ to β -Bi₂O₃ at 650 °C or δ -

Bi₂O₃ to γ- Bi₂O₃ at 640 °C [17]. A variety of deposition methods are used to produce Bi₂O₃ thin films, including reactive pulsed laser deposition[18], reactive pulsed laser deposition [19], dip coating [20], chemical vapor deposition [21], and hydrothermal synthesis [22]. The dip coating method is one of the low-cost and simple processing methods. It has attractive advantages including a nonhazardous and well suitable for deposition at low temperatures [20].

Methylene blue finds extensive usage in various applications, such as chemical indicators, pigments, biological staining, and more, primarily because of its affordability, solubility in water, and strong coloration [23]. This compound possesses an aromatic ring structure that is notably resistant to natural decomposition in water samples [24]. It is crucial to emphasize that the introduction of methylene blue (MB) into the human body can lead to severe nervous system damage [25], resulting in health concerns like eye irritation, breathing difficulties, mental disorientation, vomiting, and excessive perspiration [26].

To promote the photocatalytic activity of Bi₂O₃, Wu Xiaohong et al. demonstrated that Bi₂O₃ thin films obtained through a Sol-gel synthesis route and deposited via dip-coating method showed photocatalytic activity in the degradation of Rhodamine B, being this property related to the different temperatures applied during thermal treatment under UV visible irradiation [14]. H. Baqiah et al. studied the Effects of precursor concentration on the microstructural, optical and photoelectrochemical properties of Bi₂O₃ films synthesized by sol-gel method [27]. These studies have not investigated the influence of the precursor concentration of Bi₂O₃ on the photocatalytic performance of MB using the sol-gel with dip-coating method.

Within the confines of this manuscript, we have meticulously employed the Sol-gel dip-coating technique to fabricate Bi_2O_3 thin films atop transparent glass substrates. The prime objective of this scholarly endeavor is to delve into the intricate interplay of precursor concentrations (0.1, 0.2, 0.3, and 0.4 M) and their consequential impact on the photonic prowess of the generated samples. This research embarks on an exploration of paramount significance: the measurement of the photocatalytic prowess of these films. Under the radiant of sunlight, their efficacy in the degradation of methylene blue is discerningly examined. To fully grasp the multifaceted attributes of these thin films, analytical tools are meticulously orchestrated. X-ray diffraction (XRD), energy dispersive spectroscopy (EDS), scanning electron microscopy (SEM), UV-VIS spectroscopy, profilometry, and contact angle measurement collectively contribute to unraveling the nuanced characteristics of these films.

2. Materials and methods

2.1. Preparation of Bi_2O_3 Thin Films

The following technique was used to elaborate nanostructured Bi_2O_3 films: $\text{Bi}(\text{NO}_3)_3 \cdot 5\text{H}_2\text{O}$ was dissolved in a 48.4 mL nitric acid solution (67.5% purity) with volume ratio [1:8 HNO_3 : H_2O]. Then, 4 mL of polyethylene glycol ($\text{HO}(\text{CH}_2\text{CH}_2\text{O})_{200}\text{H}$) was added to the solution, followed by 2 g of citric acid; the solution was stirred for 15 min before each addition, and then 0.2 mL of Triton X-100 ($\text{t-Oct-C}_6\text{H}_4\text{-(OCH}_2\text{CH}_2)_x\text{.OH}$, $x=9\text{-}10$) as a surfactant was added drop by drop. After that, the solution was well stirred for 3h to obtain Sol solution. The sol was heated to 60 °C for 90 min to form a gel. A schematic diagram of the sol-gel synthesis was given in **Fig. 1**.

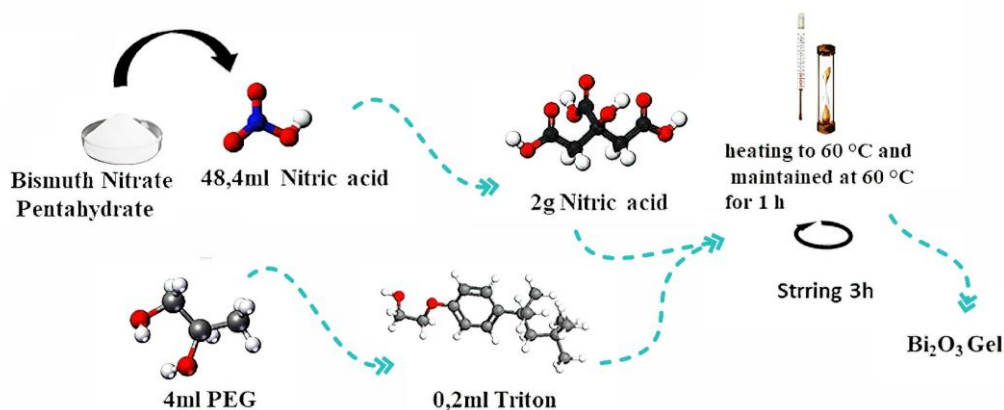


Fig .1. Schematic diagram of Bi_2O_3 preparation by sol-gel synthesis.

The solutions have been deposited on glass substrates (*MICROSCOPE SLIDES*, No. 7101), with dimensions of (7.5*2.5*0.1 cm³). Glass slides were cleaned by ultrasonic cleaning in acetone ($\text{C}_3\text{H}_6\text{O}$) and deionized water for 10 min each, then dried in open air to get well-adhered and smooth films. The weight of glass substrates was measured before and after deposition solutions to measure the thickness of samples using a sensitive balance with four digits (an analytical balance). Following that, the glass substrates were immersed in the solution for 3 min before being withdrawn at 5 cm/min and dried at 110 °C for 10 min to allow organic components to be removed. This process was repeated 10 times. The films were annealed with a heating rate of 5 °C/min for 2 h at 550 °C because the crystallization of bismuth oxides annealed at 550 °C is better than that of bismuth oxides annealed at lower temperatures due to the crystallization of the T (tetragonal) phase of bismuth oxide [28].

2.2. Film characterization:

Bi_2O_3 thin films were characterized by using different physical techniques. Bi_2O_3 crystalline structure of the samples was characterized using grazing-incidence X-ray diffractometry (*D8 Advance*) using Cu K α irradiation of wavelength 0.15405 nm in the

2 θ range of 20–80°. The crystallite size micro strain and dislocation density of the samples determined XRD from spectrum peak broadening.

The 3D surface topography and surface roughness were assessed using a Tencor P-7 mechanical profilometer, which was operated under standard environmental conditions at room temperature. This evaluation utilized the 2-bar method with a customized filter adjustment, specifically employing a Gaussian filter with a cut-off value of 0.800 μm , while addressing edge effects as well.

The surface morphology and elemental composition were obtained by field emission scanning electron microscopy (*JEOL JSM 5800*) combined with energy dispersive X-ray (EDX) analysis. The surface roughness of the samples was measured by profilometer (*Tencor P-7*).

Thickness measurement was carried out with the gravimetric weight difference method. The transmittance and absorbance spectra were recorded in UV–VIS spectrophotometer (*Jasco V-770*) over the 300–900 nm wavelength range. And contact angle measurements are performed via the sessile drop method with IC software.

2.3. Contact angle measurement

The contact angle measurement reflects the ability of a liquid to spread over a surface by wettability. The contact angles of water drop for various bismuth thin films were measured at room temperature in ambient atmosphere by homemade method. Micropipette (*SCILOGEX-iso 9001/13485*) was used to meticulously measure the volume of each drop (10 μl), and the distance between micropipette needle and the sample was fixed at 7 mm. All contact angles were averaged from five measurements with a standard deviation of approximately 5%. The average value of each drop contact

۱۱۲
۱۱۳
۱۱۴
۱۱۵
۱۱۶
۱۱۷
۱۱۸
۱۱۹
۱۲۰
۱۲۱
۱۲۲
۱۲۳
۱۲۴
۱۲۵
۱۲۶
۱۲۷
۱۲۸
۱۲۹

angle was determined using IC software. **Fig. 2** describes how the average water droplet contact angle was measured using the following equation:

$$\theta_{average} = (\theta_1 + \theta_2)/2 \tag{1}$$

Where $\theta_{average}$ is the average angles of θ_1 and θ_2 ($^\circ$), θ_1 is the angle on the left of a water drop ($^\circ$), θ_2 is the angle on the right ($^\circ$) [3,29,30].

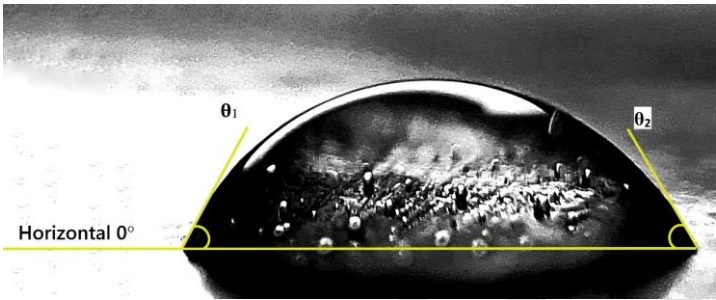


Fig. 2. The form denotes how the average value drop’s contact angle was calculated.

2.4. Preparation of the photocatalytic process for MB

The photocatalytic activities of Bi₂O₃ photocatalysts were evaluated by the photodegradation of MB dye under sunlight irradiation at ~37 °C. Each film with dimensions of (4.1*2.5*0.1 cm³) was immersed in 100 ml of MB solution (2 mg/L) for 1h in the dark to reach the adsorption-desorption equilibrium between Bi₂O₃ particles and MB, then exposed to sunlight with stirring for 4 hours. After that, a 5 ml sample was extracted from each suspension at regular intervals (1h) using syringe filter during the irradiation. After collecting the samples, we recorded UV-vis transmittance of the samples from 300 to 800 nm to measure the degradation of methylene blue [31].

3. Results and discussion

Table 1. Data analysis summary

	Unit	Thin films with different precursor concentrations
--	------	--

		0.1M	0.2M	0.3M	0.4M
Crystallographic dominant Phase		β -Bi ₂ O ₃	β -Bi ₂ O ₃	β -Bi ₂ O ₃	β -Bi ₂ O ₃
Crystal Size	nm	28.6	48.6	41.3	31.8
Surface Roughness (Rq)	nm	18.3	18.4	12.4	8.73
Film Thickness	nm	~40	~73	~83	~115
Transmission in Visible range	%	78	68	68	63
Optical direct Band Gap	eV	3.34	3.41	3.53	3.33
Optical Indirect Band Gap	eV	2.99	3.1	3.24	2.97
Bi Content	wt. %	18.41	22.33	23.27	31.04
O Content	wt. %	34.73	29.88	30.53	27.48
Si Content	wt. %	46.87	47.80	46.20	40.29
Average contact angle	°	51.37±2.13	45.57±2.68	67.14±3.66	61.61±3.21
MB degradation	%	~99	~96	~95	~93
Constant rate		1.00	0.81	0.76	0.71

3. 1. X-ray Diffraction

XRD technique was used to analyze the structure property of the films. The recorded XRD patterns of the deposited thin films are shown in **Fig. 3(a)**. Moreover, XRD patterns showed that the common structure is corresponding to Tetragonal (T) phase. The films (0.1, 0.2, and 0.3 M) mainly consist of monoclinic and tetragonal phases, which are labeled M and T, respectively. At 0.4 M film, a new peak appeared corresponding to cubic phase, which has been reported by Wu Xiaohong et al. [14]. The average crystallite size of the Bi₂O₃ thin films was estimated using the full width at half maximum (FWHM) from the line broadening of the tetragonal orientation. The average crystallite sizes were calculated using the Scherrer formula.

$$D = k \lambda / \beta \cos \theta \quad (2)$$

where D is the crystal diameter, k is the Scherrer constant and is taken equal to 1, λ is the wavelength of the X-rays, and β is the full width at half maximum (FWHM) of X-ray diffraction peaks in radians [32]. The average crystallite size of the Bi₂O₃ films

prepared by molar precursors of 0.1, 0.2, 0.3, and 0.4 M was found to be 506, 480, 407, and 360 nm, respectively.

$$(\epsilon) = \beta \cos \theta / 4. \pi \quad (3)$$

The dislocation density (δ), which represents the defects amount in the sample, is defined as the length of dislocation lines per unit volume of the crystal [33], and is calculated using the following relation [34]:

$$(\delta) = 1/D^2 \quad (4)$$

The structural parameters such as crystallite size, strain ($\epsilon_{\text{average}}$), and dislocation density (δ_{average}) are listed in **Table 2**. The variation of these parameters was function of the molar precursor, as shown in **Fig. 3(b)**.

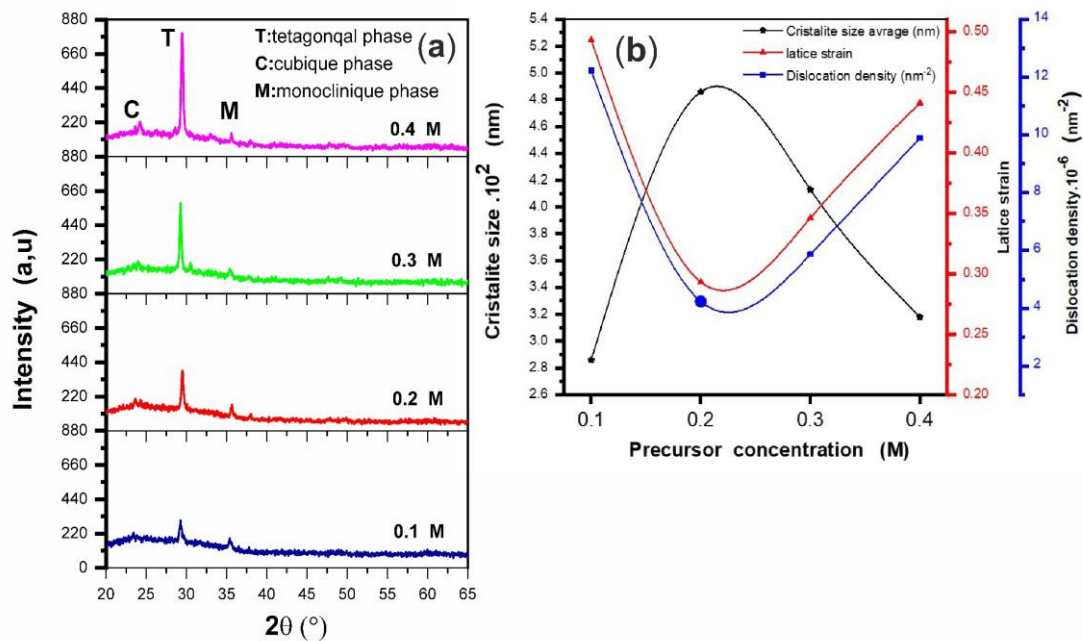


Fig. 3. (a) XRD spectra of bismuth oxide films prepared by different precursor concentrations. **(b)** The variation of crystallite size, lattice strain, and dislocation density as a function of molar concentration of precursor.

It was noticed that the crystallite size varies (from 286 to 486 nm) has inverse relation with the full width at half maximum FWHM. The small value of (δ) obtained in the present study confirmed the good crystallinity of the Bi_2O_3 thin films [35]. There is a direct correlation between dislocation density (from $9.88.10^{-6}$ to $1.22.10^{-5}$) FWHM as well as strain, since the more strain creates more dislocations in the structure of the crystal. This result is in agreement with the previously reported [36].

Tables 2. The structural parameters of various concentration precursor Bi_2O_3 thin films.

<i>Precursor concentration</i>	<i>Position $2\theta(\text{deg})$</i>	<i>d spacing</i>	<i>FWHM $B_T(\text{deg})$</i>	<i>D(nm)</i>	<i>δ dislocation density (nm^{-2})</i>	<i>ε lattice strain</i>
<i>0.1M</i>	29.28	3.05	0.29	286	$1.22.10^{-5}$	0,49
<i>0.2M</i>	29.51	3.06	0.17	486	$4.23.10^{-6}$	0,29
<i>0.3M</i>	29.27	3.05	0.20	413	$5.86.10^{-6}$	0,34
<i>0.3M</i>	29.43	3.03	0.26	318	$9.88.10^{-6}$	0,44

3.2. Bi_2O_3 thin films morphological and 3D surface topography

The surface morphology of Bi_2O_3 films (from 0.1 to 0.4 M) was carried out using Scanning Electron Microscope (SEM), as shown in **Fig. 4(a–d)**, respectively. All the films have irregular island morphology with good overall coverage. **Fig. 4a** shows isolated islands that are not clustered with each other. When the precursor concentration is increased, the island grains size increase, this is due to agglomeration in thicker film resulting grains growth as shown in **Fig. 4(b)** and slightly decreases until the film surface appears as big grains that are more compact and denser, as shown in **Fig. 4(d)**.

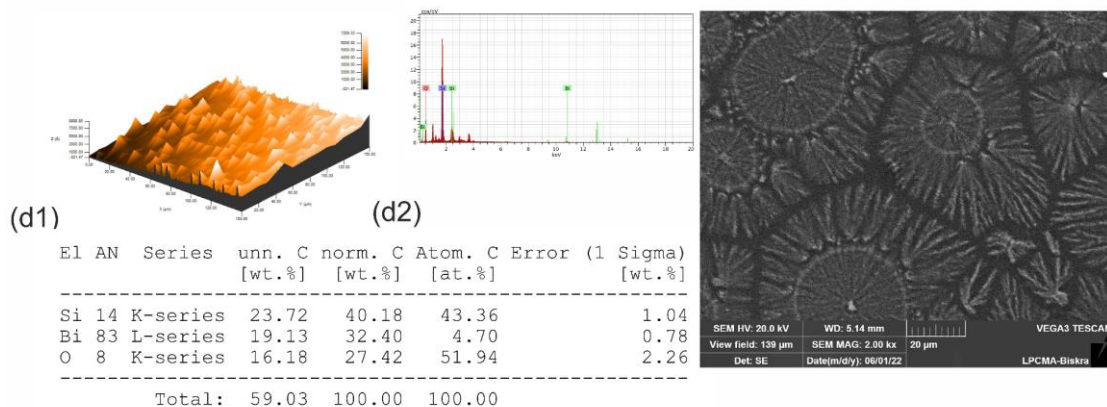
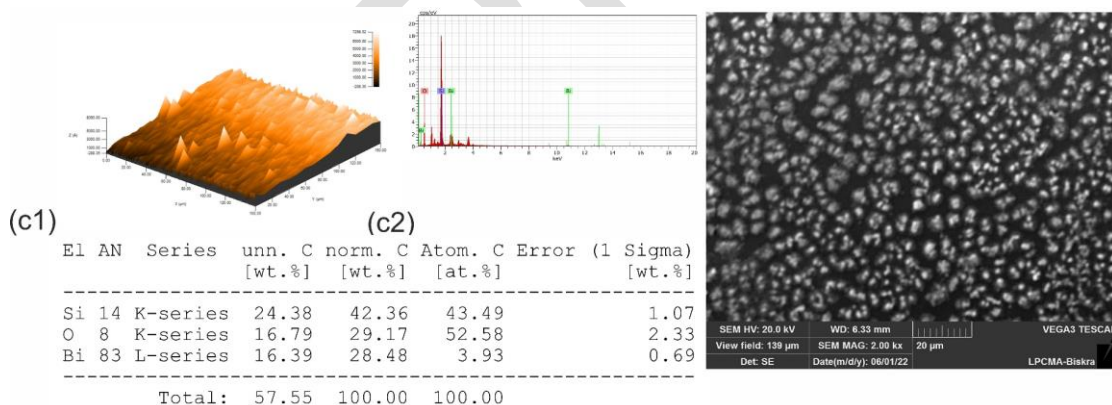
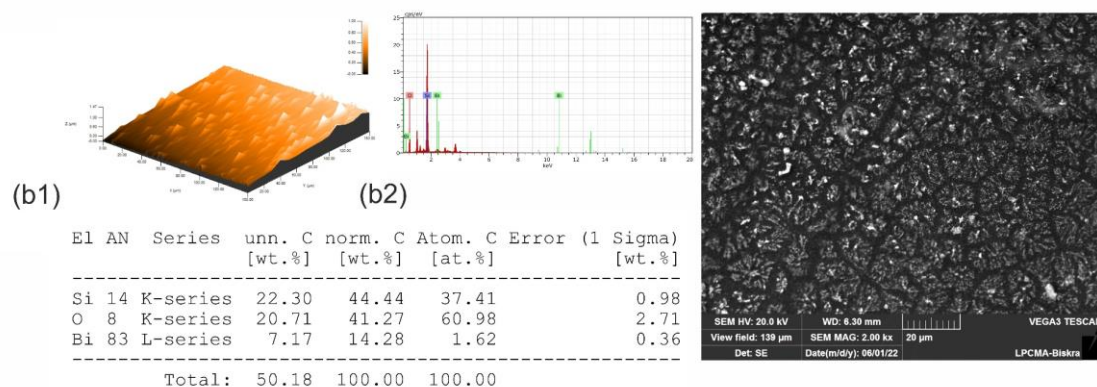
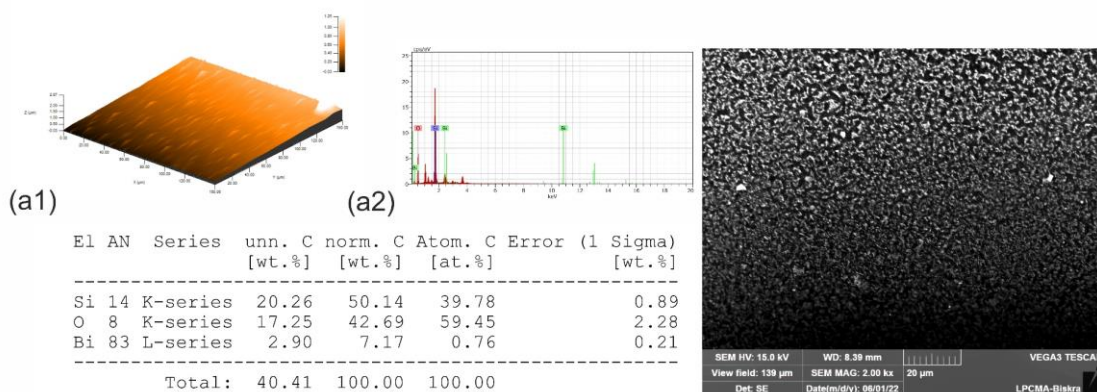


Fig. 4. SEM images and EDS spectrums of Bi₂O₃ films synthesized by the different precursor concentrations: (a2) 0.1, (b2) 0.2, (c2) 0.3, and (d2) 0.4 M.

The result of cross-sectional SEM images supports the XRD patterns that increasing the intensity of all diffraction peaks are influenced by the thickness of film. Which is good agreement with reported [37]. A quantitative analysis of the surface topography was performed from the data obtained by stylus profilometry. The investigated parameters include the average roughness, Ra, which is the arithmetic average height from a mean line over some evaluation length L; the second parameter is the root-mean-square roughness, Rq, indicating the geometric average height measured from a mean line within sampling length L; Rt denotes the third parameter and corresponds to the distance between the highest peak and deepest valley of the profile within the evaluation length L) [38]. The roughness parameters Ra, Rq, and Rt of different precursor concentrations are shown in **Table 3**. **Figs. 4** and **5** indicates that Rq values ranged from 8.73 to 18.3 nm, which are slightly higher than Ra (6.66 to 14.2 nm) values, indicating that the average amplitude from the mean line is higher than the average of peaks and valleys in the height direction.

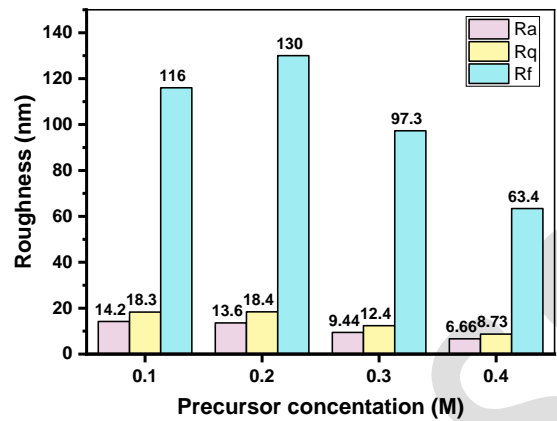
Table 3. 3D surface topography roughness analysis and shape parameters for Bi₂O₃ thin films.

<i>Roughness profile (nm)</i>	<i>Precursor concentration (M)</i>			
<i>Parameters</i>	0.1	0.2	0.3	0.4
<i>Rt (nm)</i>	116	130	97.3	63.4
<i>Rq (nm)</i>	18.3	18.4	12.4	8.73
<i>Ra (nm)</i>	14.2	13.6	9.44	6.66

The highest roughness values (18.4 and 18.3 nm) correspond to the compounds deposited with 0.2 and 0.1M films, which increase the photocatalytic efficiency. The

۱۹۷
۱۹۸
۱۹۹

lower roughness values were 9.44 nm and 6.66 nm, corresponding to 0.3 and 0.4 M films. Larger surface grains of prepared films engendered a rougher surface feature. Similarly, a substantially increased surface grain size, as reported in the ZnO film [39].



۲۰۰
۲۰۱
۲۰۲

Fig. 5. The roughness parameters Ra, Rq, and Rt of Bi₂O₃ films prepared at various molar concentrations.

۲۰۳

3.3. Bi₂O₃ thin films EDS analysis patterns

۲۰۴
۲۰۵
۲۰۶
۲۰۷
۲۰۸
۲۰۹
۲۱۰
۲۱۱

The EDS compositional analysis of bismuth thin films at different precursor concentrations is shown in **Fig. 4(a–d)**, respectively. This spectrum confirms the presence of Bi and O elements in the films. The results also indicate the presence of Si, which is attributed to the substrate glass used [40]. The Bi content increases (from 18.48 to 27.48 wt. %) as the molar concentration increases from 0.1 to 0.4 M, which is attributed to rise in its atomic percentage. Whereas the decrease in oxygen content (from 34.73 to 27.48 wt.%) could be due to the chemisorbed oxygen from the atmospheric air [41].

۲۱۲

3.4. Spectral analysis UV-visible

۲۱۳ The optical properties of Bi₂O₃ thin films prepared by using various precursor
 ۲۱۴ concentrations were studied by UV–visible spectrophotometer in the range of 300–900
 ۲۱۵ nm at room temperature, is depicted in **Fig. 7(a)**. As noticed, the transmittance increases
 ۲۱۶ with increasing wavelength, and its average value in the visible region of the spectrum
 ۲۱۷ is (78, 67.66%, 67.68%, and 63%); in the ultraviolet region, it is (51, 32, 34%, and
 ۲۱۸ 18%), with rising precursor concentrations (from 0.1 to 0.4 M), respectively. The
 ۲۱۹ transmittance can be associated with the values of grain size, RMS, porosity, and
 ۲۲۰ thickness of the films. It is generally expected that increased thickness and surface
 ۲۲۱ roughness lead to reduced transmittance, while decreasing porosity and grain size
 ۲۲۲ decrease transmittance [42]. The gravimetric weight differential method (weight
 ۲۲۳ increase method) was used to determine the thickness of the Bi₂O₃ films.

$$D = \Delta m / A \cdot \rho \quad (4)$$

۲۲۵ Where Δm is the mass difference in grams, A is the area of deposited films in cm², and
 ۲۲۶ ρ is the density of the deposited material (Bi₂O₃= 9.17 g/cm³) [43] . **Fig. 7(d)** shows the
 ۲۲۷ average thickness variation as a function of concentration precursor values. The film
 ۲۲۸ thickness increased (from 40 to 115 nm) as the precursor concentration increased (from
 ۲۲۹ 0.1 to 0.4 M); this is due to the high viscosity of the solution. The absorption coefficient
 ۲۳۰ α of the mentioned films was obtained via the following equation:

$$\alpha = \ln I_0 / I \cdot 1/d \quad (5)$$

۲۳۲ Where, d is film thickness, and I_0/I is the ratio of incident beam intensity to emergent
 ۲۳۳ beam [17][30]. Band gap values are calculated from absorption spectra, and the method
 ۲۳۴ was described in previous literature [45]. The data were analyzed using the following
 ۲۳۵ classical relationship for optical transitions:

$$(\alpha h\nu)^2 = A(h\nu - E_g)^n \quad (6)$$

Where α , h , ν , E_g , and A are the absorption coefficient, Planck constant, light frequency, band gap energy, and a is constant, respectively [46,47]. There are two types of band gaps: direct band gaps and indirect band gaps; an electron can emit a photon directly in a direct band gap but not in an indirect band gap because the electron must pass through an intermediate state to transfer momentum to the crystal lattice [46]. The estimated direct and indirect transition band-gap values are demonstrated in **Fig. 7(c1, c2)**, which show the variation of direct and indirect band-gap values with different precursor concentrations. Both the direct and indirect band gap energies increased as the precursor concentration increased from 0.1 to 0.3 M, and then they decreased at 0.4M, these results were related to the transmittance of the films. The direct and indirect band gaps of the Bi_2O_3 films with precursor concentrations of 0.1 and 0.4 M were the lowest; on the other hand, 0.2 and 0.3M are the highest. The extinction coefficient (k) can be obtained from the relation [48] :

$$K = \alpha\lambda / 4.\pi \quad (7)$$

The variation of extinction coefficient with wavelength was shown in **Fig. 7(b)**. The extinction coefficient was high in the 300–400 nm range and low in the 400–900 nm range. The rise in the extinction coefficient is directly related to absorption of light.

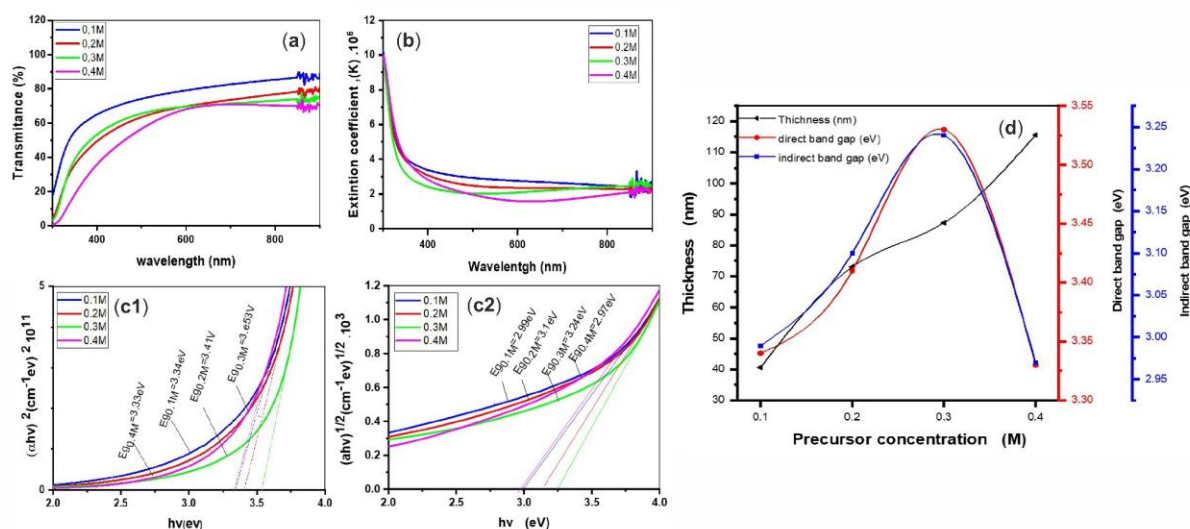


Fig. 7. (a) Optical transmittance spectrum of Bi_2O_3 synthesized by the different precursor concentrations. (b) Variation of extinction coefficient (k) versus wavelength with various molar concentrations. (c1) Direct and (c2) indirect band gap of the Bi_2O_3 films. (d) Variation of thickness and band gap with different precursor concentrations.

3.5. Wettability analysis

The wetting behavior of a solid surface in contact with water is determined by the interfacial tension between the surrounding medium (usually air) and water. When a surface exhibits high wettability, it tends to have a low contact angle, indicating that it is hydrophilic in nature and readily interacts with water. Conversely, when the wettability is low, the contact angle is high, suggesting that the surface is hydrophobic and repels water [43,49]. In the case of Bi_2O_3 films, as depicted in **Fig. 8**, water contact angle measurements were conducted.

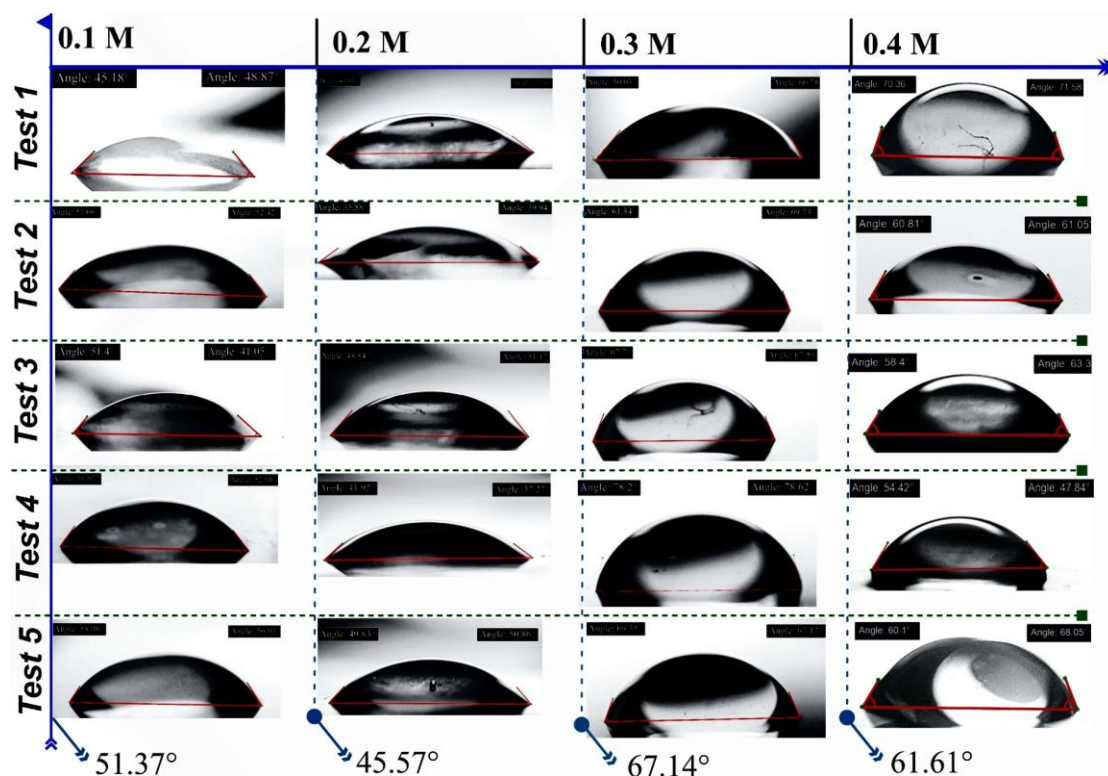


Fig. 8. Contact angles measurements images of Bi_2O_3 thin films.

The average contact angles for the samples with concentrations of 0.1 M, 0.2 M, 0.3 M, and 0.4 M were found to be 51.37°, 45.57°, 67.14°, and 61.61°, respectively, as illustrated in **Fig. 9**.

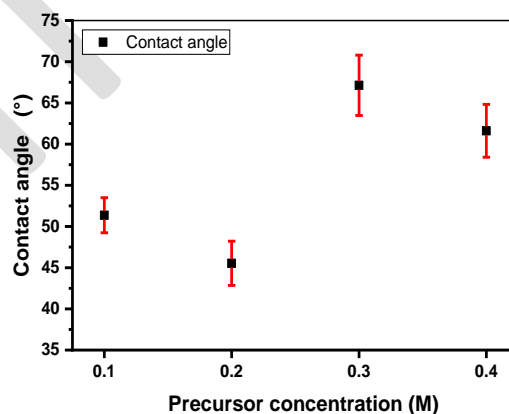


Fig. 9. Average contact angles of distilled water (H_2O) on the Bi_2O_3 substrates.

These results indicate that all the films exhibit a hydrophilic nature, implying that they have a strong affinity for water. This hydrophilic property facilitates the interaction

of the photocatalysts with contaminants in water, leading to improved degradation performance [50].

3.6. The photocatalytic efficiency

The photocatalytic efficiency of Bi₂O₃ thin films synthesized with variable precursor concentrations was evaluated by MB (2 ppm) photobleaching in an aqueous solution.

Table. 4 shows the variation of temperature, wind, and humidity for each hour. **Fig. 10(a)** shows the time-dependent visible light photocatalysis of thin films (0.1, 0.2, 0.3, 0.4 M) which decomposes the MB dye with a total exposure time of 4 h.

Table 4. Change in temperature, wind, humidity, and the amount of solar radiation per hour in the BM degradation test (Biskra, Algeria) on 20 April 2021.

<i>Time (h)</i>	0	1	2	3	4
<i>Day temp (C⁰)</i>	25	26	27	27	28
<i>Wind speed (km/h)</i>	12	11	10	9	9
<i>Humidity (%)</i>	41	40	38	37	35
<i>Radiation amount</i>	moderate				

The absorbance edge of MB dye at 664 nm was decreased with increasing sunlight irradiation time.

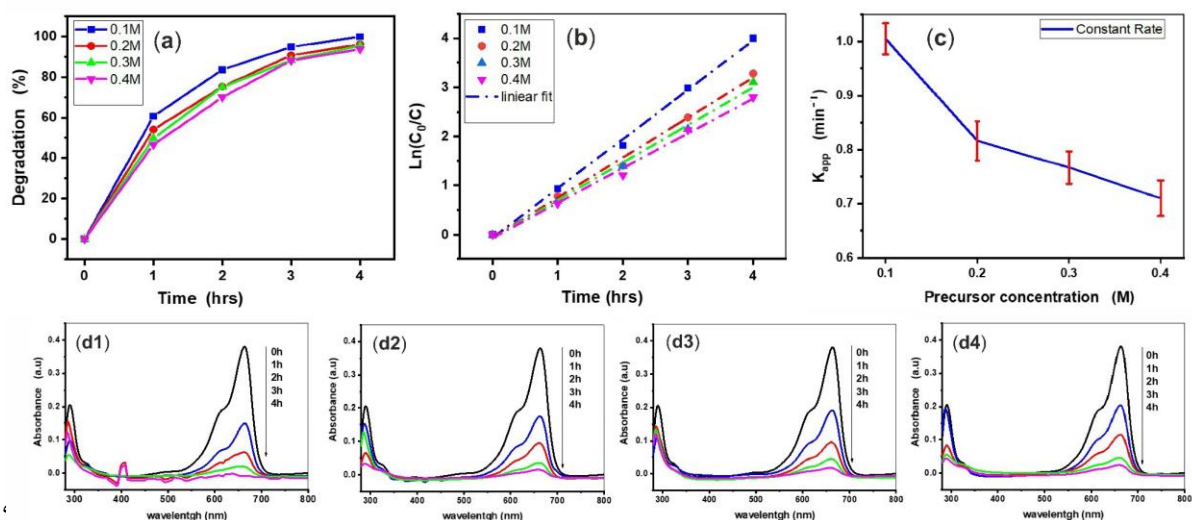


Fig. 10. (a) The degradation rate of MB dye by Bi_2O_3 thin films. (b) Photocatalytic kinetics for the all Bi_2O_3 thin films. (c) Effects of varying precursor concentrations of Bi_2O_3 thin films on MB removal under irradiation time. Absorbance spectra of the MB solutions by Bi_2O_3 thin films prepared with different precursor concentrations: (d1) 0.1, (d2) 0.2, (d3) 0.3, and (d4) 0.4 M.

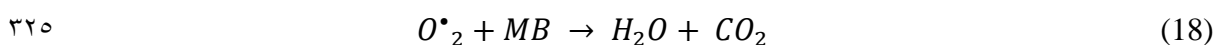
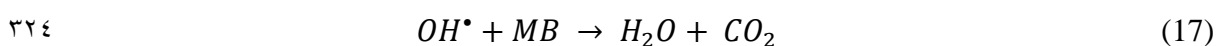
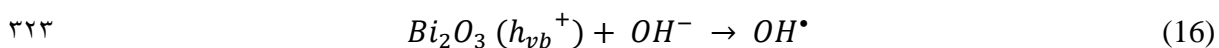
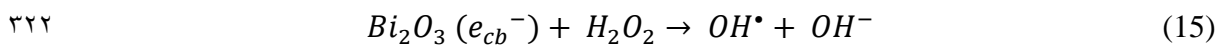
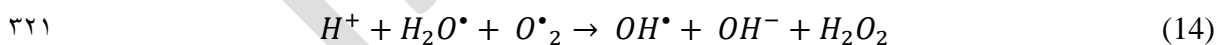
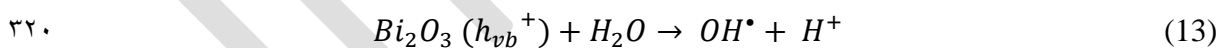
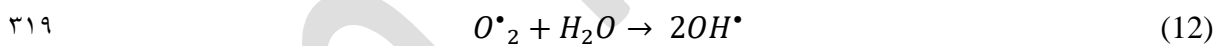
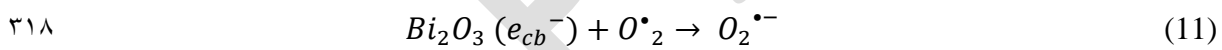
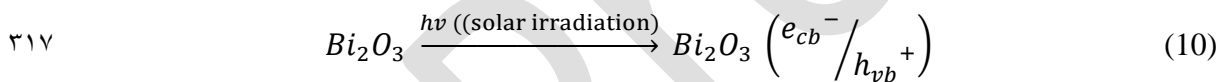
The degradation rate of MB dye is revealed in the presence of thin films as a catalyst. The following equation was used to calculate the photo degradation rate: [51]

$$D = A_0 - A_t / A_0 * 100 \% \quad (8)$$

Where A_0 is the initial absorbance at time $t = 0$ h, A_t is the absorbance after time t . The absorbance of MB dye over the Bi_2O_3 thin films under sun irradiation for 4 h is shown in **Fig. 10(d(1, 2, 3, and 4))**. It was observed that after 2h the relative amounts of MB decomposed by photocatalysis were 47.09, 49.47, 53.97, and 83.60 % when Bi_2O_3 synthesized at 0.1, 0.3, 0.4, and 0.5 M was used as photocatalyst, respectively. Bi_2O_3 thin films prepared at 0.1M have the highest photocatalytic efficiency among all samples, with 99.9 % at 4 h irradiation time. The kinetics of the photocatalytic degradation process can be generally explained by the L-H kinetic mode. [52]

$$\ln(C_0/C_t) = kt \quad (9)$$

Where C_0 is the concentration at time t_0 , C_t is the concentration at particular irradiation time, and k is the apparent pseudo-first-order rate constant (min^{-1}). The apparent rate constant (k) was successfully calculated from the slopes of the straight line obtained from the plot of natural logarithm by plotting the $\ln(C_0/C_t)$ vs irradiation time [31]. The plot of $-\ln(C/C_0)$ as a function of irradiation time for films Bi_2O_3 prepared by different precursor molarities is presented in **Fig. 10(b)**. **Fig. 10(c)** shows kinetic rate of degradation of the dye solutions with increasing amounts of bismuth precursor. As observed, the highest kinetic rate decreases with increasing molar precursors, so the highest rate 99.9% is exhibited by 0.1 M. The following equations outline the photocatalytic attributes of Bi_2O_3 films within an MB solution under sunlight [53–55]:



When bismuth oxide is activated with visible light ($\lambda \geq 420$ nm), electrons are promoted from the valence band to the conduction band, generating an electron/hole pair (e⁻/h⁺). (Eq. (10)) which are strong oxidizing and reducing agents, as shown in **Fig. 11** [56]. **Table 5** presents a thorough comparative examination between the current study and various other research papers that have incorporated thin films and powders as a pivotal element in their investigations assessing the efficacy of photocatalysts in organic dye degradation.

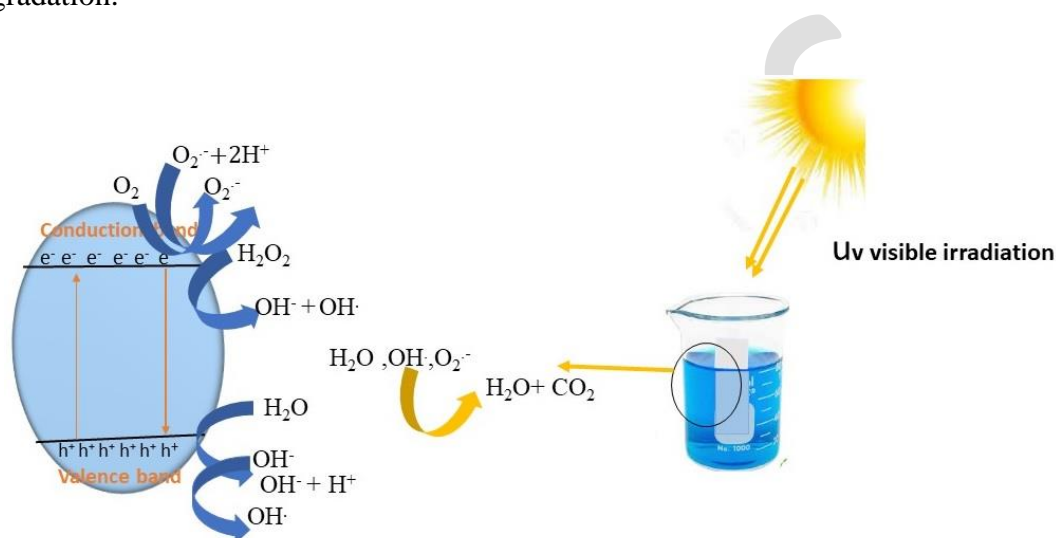


Fig. 11. Illustrates the photocatalytic mechanisms of Bi₂O₃ films for MB degradation under sunlight irradiation.

The photo-induced holes are powerful oxidizers because of their attraction for electrons. They oxidize the adsorbed water molecule or hydroxide ion to produce hydroxyl radicals (**Eq. 13**). On the other hand, the electron from the photoexcitation attacks the oxygen (**Eq. 11**), it can be reduced to the different oxygen activated species (**Eq. 11**), Then all these highly oxidizing species (•OH, •OH, H₂O₂, etc.) are capable of oxidizing organic molecules, such as MB into simpler molecules such as CO₂, H₂O [57,58].

۳۴۳ **Table 5.** Illustrates a comparison between the photocatalytic efficiency of organic dye
 ۳۴۴ degradation observed in this investigation and findings from other studies.

<i>materials</i>	<i>Dye type and concentration</i>	<i>Technique type</i>	<i>Degradation (%)</i>	<i>Time (min)</i>	<i>Irradiation Source</i>	<i>Reference</i>
β -Bi ₂ O ₃ (0.1M), Thin film	Methylene blue, 0.002 g/l	Dip-coating (glass Substrate)	~99	240	Visible light	Current study
β -Bi ₂ O ₃ , Thin film	Methylene blue, 10 ⁻⁶ mol/l	Spin-coating Deposition (Pt-coated silicon substrates)	~100	1440	Solar lamp (Ultra-Vitalux 300 W, Osram)	[59]
β -Bi ₂ O ₃ , Powder	RhB, 5 mg/L	Situ chemical transformation method	~7	25	Xe lamp (350 W)	[60]
BiOBr, Powder	RhB, 5 mg/L	Situ chemical transformation method	~30	25	Xe lamp (350 W)	[60]
Co ₃ O ₄ (Co-3) , Thin film	Methylene orange, 0.01 g/l	Nebulizer spray (glass and FTO Substrate)	~57	180	Tungsten Halogen lamp of 300 W (1 > 400 nm)	[61]
Co ₃ O ₄ (withdrawn speed of 5 mm/s) , Thin film	Methylene blue, 0.002 g/l	Dip-coating (glass Substrate)	~77	240	Visible light	[62]
CuO/ZnO (simple A) , Thin film	Methylene blue, 0.005 g/l	Spin-coating with Glass Substrate	~44	120	Xe lamp of 150 W	[63]
ZnO, Thin film	Methylene blue, 0.003 g/l	Spraying (glass Substrate)	~80	360	Visible light	[64]
CoTiO ₃ /Co ₃ O ₄ , Thin film	Indo Light Blue, 0.01 g/l	Doctor blade and spin coating (glass Substrate)	~29	60	Hg lamp of 250 W	[65]
Cu:Co (30:70) , Thin film	Methylene blue, 0.003 g/l	Dip-coating (glass Substrate)	~49	240	Visible light	[7]

۳۴۵

356 4. Conclusion

357 In this study, Bi_2O_3 films are deposited by sol-gel technique. The structural,
358 morphological, optical, and photocatalytic properties of Bi_2O_3 thin films were
359 investigated as a function of precursor concentrations. The films are polycrystalline
360 with tetragonal structure peak as a preferred orientation. The crystallite size of Bi_2O_3
361 films was not gradually affected by the change in precursor concentration or film
362 thickness. The morphology of the Bi_2O_3 surface indicates irregular and good overall
363 coverage, which increase with increasing molar precursor concentration, which is
364 supported by R_q area roughness of the sample. The optical spectrum shows that the
365 transmission increases with decreasing precursor concentration, and the maximum
366 average value of about 78 % in the visible region is observed for film prepared with 0.1
367 M. The direct band-gap values varied between 3.33 and 3.53 eV, and the direct band
368 gap varied between 2.97 - 3.24 eV when the precursor concentration was from 0.1 to
369 0.4 M. The average contact angles. Measurements proved the hydrophilic nature of the
370 films as contact angle between 51.37° and 61.61° . The degradation of MB decreases
371 with the increase in precursor concentration, and the kinetic rate of degradation and
372 degradation rate also have the highest values among all the thin films. Thus, the Bi_2O_3
373 thin film of 0.1M shows the fastest apparent photocatalytic reaction rate MB, at 99.9%,
374 corresponding to 39.7 nm crystal size, 2.01 eV band gap energy, 55 nm surface
375 roughness, and 51.37° contact angle. From the above results, it can be concluded that
376 this Bismuth oxide film is a good photocatalyst for water purification.

377 Declarations

378 Competing interests

۳۶۹ The authors report that there are no interests of a financial or personal nature in this
۳۷۰ work.

۳۷۱ **Ethical approval**

۳۷۲ Not applicable.

۳۷۳ **Informed consent**

۳۷۴ Not applicable.

۳۷۵ **Authors' contributions**

۳۷۶ All of the authors have studied this work.

۳۷۷ **Funding**

۳۷۸ The authors have reported that they did not receive any funding.

۳۷۹ **Availability of data and materials**

۳۸۰ The statement regarding the datasets used in this work can be accessed through the
۳۸۱ corresponding author.

۳۸۲ **References**

- ۳۸۳ 1. Kiwaan, H. A., Atwee, T. M., Azab, E. A., El-Bindary, A. A., "Photocatalytic degradation
۳۸۴ of organic dyes in the presence of nanostructured titanium dioxide." *J. Mol. Struct.*,
۳۸۵ 2020, 1200, 115-127.
- ۳۸۶ 2. Gamal Hasan, G., Khelef, A., Chaabia, N., Ali Mohammed, H., Laid Tedjani, M.,
۳۸۷ Althamthami, M., "Fabrication and characterization of NFMA/FTO electrochemical
۳۸۸ thin film by electrodeposition and immersion techniques: An effective detector for
۳۸۹ H₂O₂ and sunlight-driven MB degradation." *J. Photochem. Photobiol. A Chem.*, 2023,
۳۹۰ 445, 112-115.
- ۳۹۱ 3. Hasan, G. G., Mohammed, H. A., Althamthami, M., Khelef, A., Laouini, S. E.,
۳۹۲ Meneceur, S., "Synergistic effect of novel biosynthesis SnO₂@Fe₃O₄ nanocomposite:

- 393 A comprehensive study of its photocatalytic of Dyes & antibiotics, antibacterial, and
394 antimutagenic activities." *J. Photochem. Photobiol. A Chem.*, 2023, 443, 114-874.
- 395 4. Omidvar, A., Jaleh, B., Nasrollahzadeh, M., "Preparation of the GO/Pd nanocomposite
396 and its application for the degradation of organic dyes in water." *J. Colloid Interface*
397 *Sci.*, 2017, 496, 44–50.
- 398 5. Nuengmatcha, P., Porrawatkul, P., Chanthai, S., Sricharoen, P., Limchoowong, N.,
399 "Enhanced photocatalytic degradation of methylene blue using
400 Fe₂O₃/graphene/CuO nanocomposites under visible light." *J. Environ. Chem. Eng.*,
401 2019, 7, 103-438.
- 402 6. Yang, L., Chen, C., Hu, Y., Wei, F., Cui, J., Zhao, Y., Xu, X., Chen, X., Sun, D., "Three-
403 dimensional bacterial cellulose/polydopamine/TiO₂ nanocomposite membrane with
404 enhanced adsorption and photocatalytic degradation for dyes under ultraviolet-
405 visible irradiation." *J. Colloid Interface Sci.*, 2020, 562, 21–28.
- 406 7. Althamthami, M., Elhachmi, G. T., Ben Temam, H., Hasan, G. G., Rahmane, S., Gasmi,
407 B., "Effect of Different Cu:Co Film Concentrations on Photocatalytic Reactions of
408 Ethanol, MB, AMX, and Cr(VI): A Study of Film Properties & Effects of Photooxidation."
409 *J. Environ. Chem. Eng.*, 2023, 111-247.
- 410 8. Reddy, C. V., Reddy, I. N., Harish, V. V. N., Reddy, K. R., Shetti, N. P., Shim, J.,
411 Aminabhavi, T. M., "Efficient removal of toxic organic dyes and photoelectrochemical
412 properties of iron-doped zirconia nanoparticles." *Chemosphere*, 2020, 239, 124-766.
- 413 9. Akhtar, J., Tahir, M. B., Sagir, M., Bamufleh, H. S., "Improved photocatalytic
414 performance of Gd and Nd co-doped ZnO nanorods for the degradation of methylene
415 blue." *Ceram. Int.*, 2020, 46, 11955–11961.
- 416 10. Kumari, V., Mittal, A., Jindal, J., Yadav, S., Kumar, N., "S-, N- and C-doped ZnO as
417 semiconductor photocatalysts: A review." *Front Mater Sci.*, 2019, 13.
- 418 11. Kabra, K., Chaudhary, R., Sawhney, R. L., "Treatment of hazardous organic and
419 inorganic compounds through aqueous-phase photocatalysis: A review." *Ind. Eng.*
420 *Chem. Res.*, 2004, 43, 7683–7696.
- 421 12. Soares, L., Alves, A., "Photocatalytic properties of TiO₂ and TiO₂/WO₃ films applied
422 as semiconductors in heterogeneous photocatalysis." *Mater. Lett.*, 2018, 211, 339–
423 342.
- 424 13. Li, J. Z., Zhong, J. B., Zeng, J., Feng, F. M., He, J. J., "Improved photocatalytic activity of
425 dysprosium-doped Bi₂O₃ prepared by sol-gel method." *Mater. Sci. Semicond.*
426 *Process.*, 2013, 16, 379–384.
- 427 14. Xiaohong, W., Wei, Q., Weidong, H., "Thin bismuth oxide films prepared through the
428 sol – gel method as photocatalyst." 2007, 261, 167–171.

15. Orozco-Hernández, G., Olaya-Flórez, J., Pineda-Vargas, C., Alfonso, J. E., Restrepo-Parra, E., "Structural, chemical and electrochemical studies of bismuth oxide thin films growth via Unbalanced Magnetron Sputtering." *Surfaces and Interfaces*, 2020, 21, 100-627.
16. Dev, B. C., Babu, M. H., Podder, J., Sagadevan, S., Zubair, A., "Low temperature synthesis of α - and β -phase Bi₂O₃ thin film via B doping: tailoring optical band gap and n- to p-type Bi₂O₃." *J. of Mater. Sci.: Mater. in Ele.*, 2019, 30, 15670–15682.
17. Dapčević, A., Poleti, D., Rogan, J., Radojković, A., Radović, M., Branković, G., "A new electrolyte based on Tm³⁺-doped δ -Bi₂O₃-type phase with enhanced conductivity." *Sol. Sta. Ion.*, 2015, 280, 18–23.
18. Fan, H. T., Pan, S. S., Teng, X. M., Ye, C., Li, G. H., Zhang, L. D., " δ -Bi₂O₃ thin films prepared by reactive sputtering: Fabrication and characterization." *Thin Solid Films*, 2006, 513, 142–147.
19. Zhu, B. L., Zhao, X. Z., "Study on structure and optical properties of Bi₂O₃ thin films prepared by reactive pulsed laser deposition." *Opt. Mater. (Amst.)*, 2006, 29, 192–198.
20. Hettal, S., Ouahab, A., Rahmane, S., Benmessaoud, O., Sayad, M., "Effect of the Number of Dips on the Properties of Copper Oxide Thin Films Deposited by Sol-Gel Dip-Coating Technique." *Iranian Journal of Materials Science and Engineering*, 2022, 19, 1–8.
21. Sun, Z., Oka, D., Fukumura, T., "Epitaxial Growth of β -Bi₂O₃ Thin Films and Particles with Mist Chemical Vapor Deposition." *Cryst. Growth Des.*, 2019, 19, 7170–7174.
22. Wu, S., Fang, J., Xu, W., Cen, C., "Hydrothermal synthesis, characterization of visible-light-driven α -Bi₂O₃ enhanced by Pr³⁺ doping." *Journal of Chemical Technology and Biotechnology*, 2013, 88, 1828–1835.
23. Tong, Y., Jiang, B., Chen, X., Ren, X., Lu, J., Ding, L., "Synergistic degradation of methylene blue by laser cavitation and activated carbon fiber." *Opt. Laser Technol.*, 2022, 155, 108-417.
24. Chen, M. L., Li, S. S., Wen, L., Xu, Z., Li, H. H., Ding, L., Cheng, Y. H., "Exploration of double Z-type ternary composite long-afterglow/graphitic carbon nitride@metal-organic framework for photocatalytic degradation of methylene blue." *J. Colloid Interface Sci.*, 2023, 629, 409–421.
25. Arif, M., Liu, G., Yousaf, B., Ahmed, R., Irshad, S., Ashraf, A., Zia-ur-Rehman, M., Rashid, M. S., "Synthesis, characteristics and mechanistic insight into the clays and clay minerals-biochar surface interactions for contaminants removal-A review." *J. Clean Prod.*, 2021, 310, 127-548.

26. El-Ghobashy, M. A., Salem, I. A., El-Dahrawy, W. M., Salem, M. A., "Fabrication of α -MnO₂/Fe-Mn binary oxide nanocomposite as an efficient adsorbent for the removal of methylene blue from wastewater." *J. Mol. Struct.*, 2023, 1272, 118-134.
27. Baqiah, H., Talib, Z. A., Liew, J. Y. C., Shaari, A. H., Zainal, Z., F, L. M., "Effects of precursor concentration on the microstructural, optical and photoelectrochemical properties of Bi₂O₃ films synthesized by sol-gel method." *Optik. (Stuttg.)*, 2020, 206.
28. Weidong, H., Wei, Q., Xiaohong, W., Hailong, N., "Thin bismuth oxide films prepared through the sol – gel method." 2007, 61, 4100–4102.
29. Althamthami, M., Guettaf Temam, E., Ben Temam, H., Hasan, G. G., Malfi, N., "Influence of hole-scavenger and different withdrawn speeds on photocatalytic activity of Co₃O₄ thin films under sunlight irradiation." *Ceram. Int.*, 2022, 48, 31570–31578.
30. Althamthami, M., Guettaf Temam, E., Temam, H. Ben, Saad, R., Hasan, G. G., "Improved photocatalytic activity under the sunlight of high transparent hydrophilic Bi-doped TiO₂ thin-films." *J. Photochem. Photobiol. A Chem.*, 2023, 443, 114-818.
31. Raza, W., Bahnemann, D., Muneer, M., "A green approach for degradation of organic pollutants using rare earth metal doped bismuth oxide." *Catal. Today*, 2018, 300, 89–98.
32. Jadhav, C. H., Pagare, P. K., Inamdar, K. K., Kadam, L. D., "Preparation of Bismuth Oxide Thin Films by Spray Pyrolysis Method and Its Characterizations." *Macromol. Symp.*, 2019, 387, 1–3.
33. Seid, E. T., Dejene, F. B., Urgessa, Z. N., Botha, J. R., "Refluxed sol–gel synthesized ZnO nanopowder with variable zinc precursor concentrations." *Appl. Phys. A Mater. Sci. Process*, 2018, 124, 1–13.
34. Ravishankar, S., Balu, A. R., Anbarasi, M., Nagarethinam, V. S., "Influence of precursor molar concentration on the structural, morphological, optical and electrical properties of PbS thin films deposited by spray pyrolysis technique using perfume atomizer." *Optik. (Stuttg.)*, 2015, 126, 2550–2555.
35. Kamble, D. L., Harale, N. S., Patil, V. L., Patil, P. S., Kadam, L. D., "Characterization and NO₂ gas sensing properties of spray pyrolyzed SnO₂ thin films." *J. Anal. Appl. Pyrolysis.*, 2017, 127, 38–46.
36. Seid, E. T., Dejene, F. B., Urgessa, Z. N., Botha, J. R., "Refluxed sol–gel synthesized ZnO nanopowder with variable zinc precursor concentrations." *Appl. Phys. A Mater. Sci. Process*, 2018, 124, 1–13.
37. Aryanto, D., Jannah, W. N., Masturi, Sudiro, T., Wismogroho, A. S., Sebayang, P., Sugianto, Marwoto, P., "Preparation and structural characterization of ZnO thin films by sol-gel method." *J. Phys. Conf. Ser.*, 2017, 817, 012-025.

38. Pérez-González, M., Tomás, S. A., Santoyo-Salazar, J., Morales-Luna, M., "Enhanced photocatalytic activity of TiO₂-ZnO thin films deposited by dc reactive magnetron sputtering." *Ceram. Int.*, 2017, 43, 8831–8838.
39. Kamaruddin, S. A., Chan, K. Y., Yow, H. K., Zainizan Sahdan, M., Saim, H., Knipp, D., "Zinc oxide films prepared by sol-gel spin coating technique." *Appl. Phys. A Mater. Sci. Process*, 2011, 104, 263–268.
40. Ravishankar, S., Balu, A. R., Anbarasi, M., Nagarethinam, V. S., "Influence of precursor molar concentration on the structural, morphological, optical and electrical properties of PbS thin films deposited by spray pyrolysis technique using perfume atomizer." *Optik. (Stuttg.)*, 2015, 126, 2550–2555.
41. Kouidri, Nabila, Rahmane, Saâd, "Effect of Cobalt Chloride Concentration on Structural, Optical and Electrical Properties of Co₃O₄ Thin Films Deposited by Pneumatic Spray." *Journal of New Technology and Materials*, 2020, 10, 56–62.
42. Sbeta, M., Atilgan, A., Atli, A., Yildiz, A., "Influence of the spin acceleration time on the properties of ZnO:Ga thin films deposited by sol-gel method." *J. Solgel. Sci. Technol.*, 2018, 86, 513–520.
43. Shaikh, A. A., Waikar, M. R., Sonkawade, R. G., "Effect of different precursors on electrochemical properties of manganese oxide thin films prepared by SILAR method." *Synth. Met.*, 2019, 247, 1–9.
44. Guettaf Temam, E., Djani, F., Rahmane, S., Ben Temam, H., Gasmi, B., "Photocatalytic activity of Al/Ni doped TiO₂ films synthesized by sol-gel method: Dependence on thickness and crystal growth of photocatalysts." *Surfaces and Interfaces*, 2022, 31, 077-102.
45. Xiaohong, W., Wei, Q., Li, L., Yun, G., Zhaoyang, X., "Photocatalytic property of nanostructured Fe³⁺-doped Bi₂O₃ films." *Catal. Commun.*, 2009, 10, 600–604.
46. Qin, W., Qi, J., Wu, X., "Photocatalytic property of Cu²⁺-doped Bi₂O₃ films under visible light prepared by the sol gel method." *Vacuum*, 2014, 3–6.
47. Mokrani, N., Guettaf Temam, E., Barkat, H., Ben Temam, H., Rahmane, S., Althamthami, M., "Boosting photocatalytic stability: hydrophilic Sr-doped ZnO thin films prepared via the SILAR method for enhanced performance over multiple cycles." *Phys. Scr.*, 2024, 99, 094-095.
48. Jothibas, M., Manoharan, C., Dhanapandian, S., Jeyakumar, S. J., "Influence of precursor concentration on sprayed In₂O₃ thin films." *Asian Journal of Chemistry*, 2013, 25.
49. Althamthami, M., Temam, G., Hachmi, E. I., Temam, H. Ben, Hasan, G. G., Gasmi, B., Hasan, G., Rahmane, S., "Tailor-made Tenorite (CuO) Interface Films for Enhanced Photocatalysis: An Improved Dip-Coating Approach with Enhanced Surface Topography and Hydrophobicity." 2023, 1.

- 040 50. Lu, H., Hao, Q., Chen, T., Zhang, L., Chen, D., Ma, C., Yao, W., Zhu, Y., "A high-
041 performance Bi₂O₃/Bi₂SiO₅ p-n heterojunction photocatalyst induced by phase
042 transition of Bi₂O₃." *Appl. Catal. B*, 2018, 237, 59–67.
- 043 51. Begum, S., Ahmaruzzaman, M., "Green Synthesis of SnO₂ Nanoparticles loaded on
044 Activated Carbon and its Application as Photocatalyst in the Degradation of Alizarin
045 Red S Dye." *Mater. Today Proc.*, 2018, 5, 2314–2320.
- 046 52. Islam, M. R., Rahman, M., Farhad, S. F. U., Podder, J., "Structural, optical and
047 photocatalysis properties of sol–gel deposited Al-doped ZnO thin films." *Surfaces and
048 Interfaces*, 2019, 16, 120–126.
- 049 53. Li, J., Guo, J., Zhang, J., Sun, Z., Gao, J., "Surface etching and photodeposition
050 nanostructures core-shell Cu₂O@CuO-Ag with S-scheme heterojunction for high
051 efficiency photocatalysis." *Surfaces and Interfaces*, 2022, 34, 102-308.
- 052 54. Tornabene, F., Triantafillou, T., Teklemariam Gaim, Y., Mekides Yimanuh, S., Girmay
053 Kidanu, Z., "Enhanced Photocatalytic Degradation of Amoxicillin with Mn-Doped
054 Cu₂O under Sunlight Irradiation." *Journal of Composites Science*, 2022, 6, 317.
- 055 55. Balarak, D., Mengelizadeh, N., Rajiv, P., Chandrika, K., "Photocatalytic degradation of
056 amoxicillin from aqueous solutions by titanium dioxide nanoparticles loaded on
057 graphene oxide." *Environmental Science and Pollution Research*, 2021, 28, 49743–
058 49754.
- 059 56. Kusuma, K. B., Manju, M., Ravikumar, C. R., Dileepkumar, V. G., Kumar, A. N.,
060 Santosh, M. S., Murthy, H. C. A., Gurushantha, K., "Probe Sonicated Synthesis of
061 Bismuth Oxide (Bi₂O₃): Photocatalytic Application and Electrochemical Sensing of
062 Ascorbic Acid and Lead." *J. Nanomater.*, 2022.
- 063 57. Zahid, A. H., Han, Q., Jia, X., Li, S., Hangjia, H., Liu, H., "Highly stable 3D multilayered
064 nanoparticles-based β -Bi₂O₃ hierarchitectre with enhanced photocatalytic activity."
065 *Opt. Mater. (Amst.)*, 2020, 109, 110-389.
- 066 58. Abu-Dief, A. M., Mohamed, W. S., " α -Bi₂O₃ nanorods: synthesis, characterization and
067 UV-photocatalytic activity." *Mater. Res. Express*, 2017, 4, 035-039.
- 068 59. Perez-Mezcua, D., Bretos, I., Jiménez, R., Ricote, J., Jiménez-Rioboó, R. J., da Silva, C.
069 G., Chateigner, D., Fuentes-Cobas, L., Sirera, R., Calzada, M. L., "Photochemical
070 solution deposition of β -Bi₂O₃ thin films." *J. Solgel. Sci. Technol.*, 2017, 81, 355–361.
- 071 60. Wu, S., Xie, Y., Zhang, X., Huang, Z., Liu, Y., Fang, M., Wu, X., Min, X., "In situ synthesis
072 of adsorptive β -Bi₂O₃/BiOBr photocatalyst with enhanced degradation efficiency." *J.
073 Mater. Res.*, 2019, 34, 3450–3461.
- 074 61. Ravi Dhas, C., Venkatesh, R., David Kirubakaran, D., Princy Merlin, J., Subramanian, B.,
075 Moses Ezhil Raj, A., "Electrochemical sensing of glucose and photocatalytic
076 performance of porous Co₃O₄ films by nebulizer spray technique." *Mater. Chem.
077 Phys.*, 2017, 186, 561–573.

62. Althamthami, M., Guettaf Temam, E., Ben Temam, H., Hasan, G. G., Malfi, N., "Influence of hole-scavenger and different withdrawn speeds on photocatalytic activity of Co₃O₄ thin films under sunlight irradiation." *Ceram. Int.*, 2022, 48, 31570–31578.
63. Xu, L., Su, J., Zheng, G., Zhang, L., "Enhanced photocatalytic performance of porous ZnO thin films by CuO nanoparticles surface modification." *Materials Science and Engineering: B*, 2019, 248, 114-405.
64. Mrabet, C., Jaballah, R., Mahdhi, N., Boukhachem, A., Amlouk, M., "CuO-ZnO nanocomposites-based thin films: Characterization, physical properties and sunlight photocatalytic degradation of organic pollutants." *J. Alloys. Compd.*, 2023, 968, 172-252.
65. Habibi, M. H., Shojaee, E., "Synthesis of a heterojunction CoTiO₃/Co₃O₄ nano-composite thin film with superior photocatalytic activity and reusability: Effect of calcination temperature on phase transformation and effect of oxidants on enhanced degradation of Indo Light Blue dye." *Spectrochim. Acta A Mol Biomol. Spectrosc.*, 2020, 229, 117-796.